Finite Elements in Analysis and Design 47 (2011) 753–763

Contents lists available at ScienceDirect

Finite Elements in Analysis and Design

journal homepage: www.elsevier.com/locate/finel

Topology optimization for nonlinear dynamic problem with multiple materials and material-dependent boundary condition

Gil Ho Yoon

School of Mechanical Engineering, Hanyang University, Republic of Korea

ARTICLE INFO

Article history:
Received 19 October 2010
Received in revised form
23 February 2011
Accepted 23 February 2011
Available online 21 March 2011

Keywords:
Topology optimization
Nonlinear eigenvalue problem
Multiple materials
Material- dependent boundary condition
Geometrically nonlinear

ABSTRACT

This article develops a new optimization scheme for geometrically nonlinear dynamic topology optimization considering multiple materials and material-dependent boundary conditions. In the framework of convectional topology optimization procedures, some major issues must be addressed regarding complicated analysis and optimization formulations for these difficult conditions, as well as the unstable elements. To rigorously resolve these issues, this article develops a new patch stacking method based on our previous contribution (the element connectivity parameterization method (ECP) and the element stacking method). Compared with existing multi-material topology optimization schemes, the two differences in the present scheme are the stacking of multiple patches of the ECP method on the same discretization pixel, and the selection of one patch or no patch among them. To show the potential usage and limitations of the developed optimization method, several topology optimization examples with the above conditions are solved.

1. Introduction

This paper develops a new optimization procedure based on a new numerical analysis scheme for a nonlinear dynamic problem involving multiple materials and the associated material-dependent boundary conditions. To systematically improve the vibration or noise characteristics of an engineered structure, size, shape, and topology optimization methods based on the finite element (FE) procedure have been developed and applied [1–11]. Because topological evolutions (creating, reshaping, and removing holes within design domains) become possible, it is generally accepted that topology optimization can provide better initial layout designs than the other two design methods. One key concept in topology optimization is that by applying mathematical optimization algorithms, the material properties of each element, such as Young's modulus and the density in a structural dynamic problem, are interpolated from those in the nonstructural domain (so-called "void") to those in the structural domain (so-called "solid") with respect to the design variables defined for each element. Depending on how the material properties are modeled with respect to the design variables, the solid isotropic material with penalization (SIMP) approach (sometimes called the density-based method) or the homogenization-based approach can be employed [2–4,10,11].

This investigation addresses the following difficult conditions for which the conventional topology optimization formulation or modeling techniques are hard to be applied.

1. Geometrically nonlinear dynamic structure with multiple materials
2. Material-dependent boundary conditions in a dynamic structure

To rigorously approach topology optimization considering the challenging conditions above, we expand the concept of the element connectivity parameterization (ECP) method combined with the element stacking method [9,12,13]. The advantage of the ECP method lies in the fact that its treatment of the unstable elements (flipped elements) is very straightforward. The unstable elements, whose areas are flipped, cause non-convergence or erratic convergence in the Newton–Raphson iteration method. Hence, it is known that special numerical treatments are required to stabilize the topology optimization process for a geometrically nonlinear structure (see Ref. [12] and references therein). Resolving this issue was the aim of our previous contribution, called the element connectivity parameterization (ECP) method [12]. Unlike the standard density topology optimization method for finding optimal material distribution, this method defines and optimizes the connectivities among solid elements. Because it does not change the material properties of solid elements, it effectively resolves the issue of unstable elements. A drawback, however, is that the ECP method uses more degrees of freedom

E-mail addresses: ghy@hanyang.ac.kr, gilho.yoon@gmail.com

0168-874X/$ - see front matter © 2011 Elsevier B.V. All rights reserved.
doi:10.1016/j.finel.2011.02.006

than conventional FE-based optimization methods. Recently, this ECP method was applied to the nonlinear dynamic problem by developing a patch mass method that defines mass matrix interpolation for the ECP method [13]. However, it is still challenging and imprecise to apply the ECP method to systems with multiple materials that have different material properties, in spite of some research into the application of existing density-based topology optimization methods to systems with multiple materials. Therefore, in this paper, we study how the ECP method can be applied to multiple materials.

In addition, we present an innovative modeling technique to implement the material-dependent boundary conditions for a dynamic problem. Such material-dependent boundary conditions may arise when only a particular material among a group of given materials is allowed along some specific boundaries (displacement or force boundary) because of assembly or mechanical/thermal impedance-matching requirements. To effectively cope with multiple materials and material-dependent boundary conditions in a dynamic problem, the element stacking method, which was researched in Ref. [13] in the framework of the standard element density method, is expanded to the present *patch stacking method* in the framework of the ECP method.

To illustrate the present patch stacking method, let us compare the different interpolation schemes for multiple materials in Fig. 1. Here the three different schemes, namely the interpolations of standard density [1], the element stacking [13], and the present patch stacking method, are used to choose one material (or layer) between the first and second material (or layer) or no material (Void). In the standard element density method, the material properties of one element, i.e., Young's moduli E_1 and E_2 and densities ρ_1 and ρ_2, here, are interpolated with respect to the design variables (γ_1 and γ_2). In the framework of the element stacking method, two physical solid state elements, i.e., the first element having E_1 and ρ_1 and the second element having E_2 and ρ_2, are juxtaposed as shown in Fig. 1(b), and an optimization algorithm can choose one of them to simulate the structural domain and neither of them to simulate a void domain. Similarly, in the framework of the present patch stacking method, the ECP patches, which consist of a solid element and zero-length links, are juxtaposed as shown in Fig. 1(c). (For a detailed description and an implementation of the ECP patch, see Ref. [17].) To determine optimal layouts, an optimization algorithm can choose one of the patches, as in the element stacking method. The advantage of this present patch stacking method lies in the fact that the material-dependent boundary condition can be assigned to the separate nodes of patches, considering the geometrical nonlinearity, which will be explained later in detail. By developing and combining the abovementioned methods, it is possible to perform topology optimization of a nonlinear dynamic system with multiple materials and material-dependent boundary conditions. To obtain a converged layout for either solids or void, a new interpolation function of the mass matrices for the ECP method is also proposed.

The layout of this paper is as follows. After describing the equations for a nonlinear dynamic system, we introduce and implement it in the framework of the ECP approach. By extending the idea of the element stacking method to the patch stacking method, it becomes possible to solve the multi-material dynamic problem. In Section 4, the topology optimization problem is formulated and the new interpolation functions for stiffness and mass matrices suitable to the developed patch stacking method are introduced. To show the potential of the proposed method, several numerical examples are considered. Finally, our findings and some topics for future research are summarized and discussed in the conclusion.

2. Nonlinear dynamic analysis using patch stacking method

2.1. Nonlinear dynamic analysis

To calculate the eigenfrequencies and the associated eigenmodes of a geometrically nonlinear structure, the modal analysis depicted in Fig. 2 should be conducted with the tangent stiffness

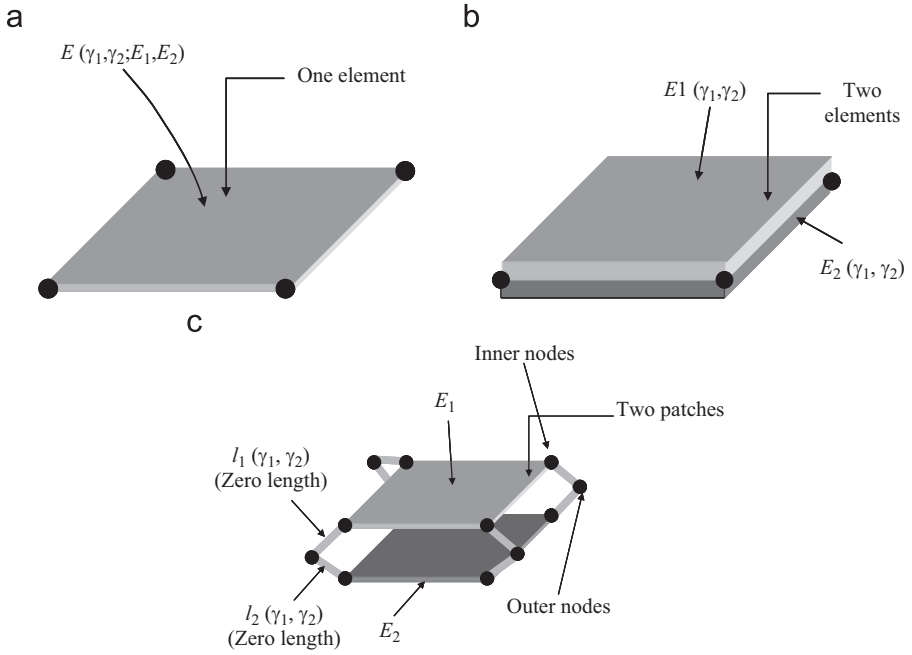

Fig. 1. Comparisons of the concepts with two materials for (a) existing multi-material+ designs, (b) the element stacking method, and (c) the present patch stacking method (patch: the basic discretizing unit in the ECP method).

matrix computed at the deformed domain for a given static load and with the displacement-independent mass matrix [14,15]. Accordingly, the eigenfrequencies of a geometrically nonlinear structure are dependent on the current static displacements, even for a structure made of a linear elastic material.

To obtain the tangent stiffness matrix, the following basic nonlinear equation is solved first:

$$^{t+\Delta t}\mathbf{R} - {}^{t+\Delta t}\mathbf{F} = \mathbf{0} \tag{1}$$

where the vectors $^{t+\Delta t}\mathbf{R}$ and $^{t+\Delta t}\mathbf{F}$ store the externally applied loads and the vector of the nodal point forces, respectively. Since the force vector $^{t+\Delta t}\mathbf{F}$ depends on the displacements nonlinearly, we should employ an iteration procedure for the solution of (1). Here, the Newton–Raphson iteration is employed for equations [14,15]

$$^{t+\Delta t}\mathbf{U}^{(k)} = {}^{t+\Delta t}\mathbf{U}^{(k-1)} + \Delta\mathbf{U}^{(k)}, \quad {}^{t+\Delta t}\mathbf{U}^{(0)} = {}^{t}\mathbf{U} \tag{2}$$

$$^{t}\mathbf{K}_{T}^{(k-1)}\Delta\mathbf{U}^{(k)} = \Re(^{t+\Delta t}\mathbf{U}^{(k-1)}) \tag{3}$$

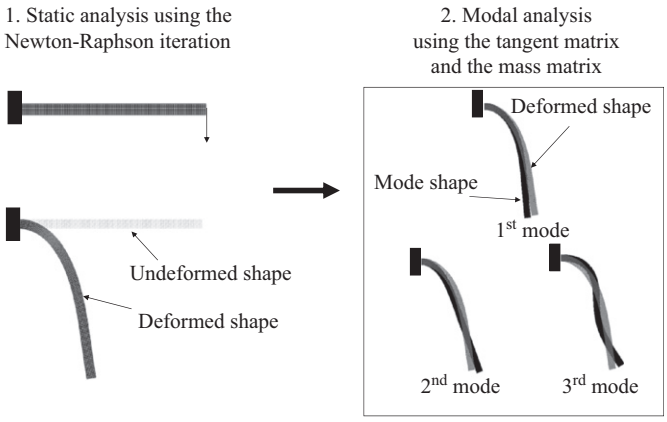

Fig. 2. Two steps of nonlinear eigenfrequency analysis.

where the superscript (k) denotes the kth iteration step in the Newton–Raphson method. The incremental residual and tangent stiffness matrix are denoted by $\Re(^{t+\Delta}\mathbf{tU}^{(k-1)})$ and $^{t}\mathbf{K}_{T}^{(k-1)}$, respectively. The updated displacements and displacements at time $t+\Delta t$ of a generic point of a body are denoted by $\Delta\mathbf{U}$ and $^{t+\Delta t}\mathbf{U}$, respectively. In each iteration at Eq. (2), we calculate in an out-of-balance load that yields an increment displacement until the incremental displacement is sufficiently small. After solving the nonlinear static Eq. (1), the eigenfrequencies are obtained through the following modal analysis. Note that the displacement-dependent tangent stiffness matrix, $^{t+\Delta t}\mathbf{K}_{T}$, and the displacement-independent mass matrices, $\mathbf{M}$, are used

$$(^{t+\Delta t}\mathbf{K}_{T} - \omega^2\mathbf{M})\Phi = \mathbf{0}, \quad \Phi^{T}M\Phi = \mathbf{I} \tag{4}$$

where ω and Φ are the angular velocity and the associated eigenmode, respectively. The identity matrix $\mathbf{I}$ is of the same size as the mass or stiffness matrix. For more details, see Refs. [14,15] and the references therein.

2.2. The patch stacking method of the ECP method for multiple materials and material-dependent boundary condition

2.2.1. Concept of the present patch stacking method

To consider multiple materials and the material-dependent boundary condition in a geometrically nonlinear structure, we expand the concept of the element stacking method [13] to the patch stacking method, as shown in Fig. 3. As explained in the preceding section, the element stacking method was introduced to consider the material-dependent boundary condition as well as multiple materials in the framework of the element density-based method. Like the element stacking method, the patch stacking method presented in this article juxtaposes several ECP patches and selects only one patch among them, or no patch for a void, by changing the stiffness values of the zero-length links. As an example, let us assume that we want to somehow design an optimal structure using two materials for the left clamped boundary condition for material 1 and the force is only applied to material 2, as shown in Fig. 3. To our knowledge, it is difficult to

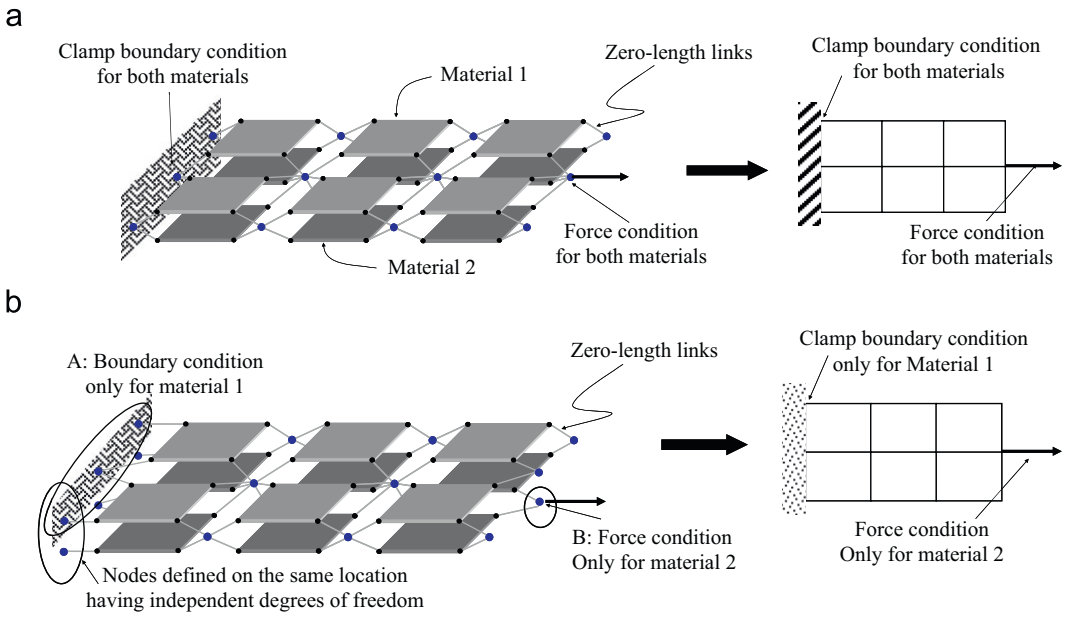

Fig. 3. (a) Patch stacking method for two materials and (b) the prescription of material-dependent boundary/loading conditions (for purpose of illustration, the two layers are separated).

find a solution to this boundary condition and it is almost impossible for nonlinear structures. We therefore devised the patch stacking method, which juxtaposes several patches and uses interpolation functions in order to select one patch or no patches. To consider the clamped boundary condition only for material 1, the method introduces new nodes at the boundary condition marked by A in Fig. 3(b) and the boundary conditions are imposed at the node consisting of the ECP patches for material 1. Similarly, only the node for material 2, denoted as B in Fig. 3(b), receives the force. In these ways, the material-dependent boundary conditions (force and displacement) that are difficult to implement in the standard FE procedure can be considered.

2.2.2. Static nonlinear analysis

To derive discretized FE equations for a nonlinear dynamic structure, the eth patch shown in Figs. 4 and 5 is first considered, along with the assumption of geometrical nonlinearity. As our notation conventions for the ECP patch, the nodes connecting plane elements, which do not interpolate their material properties during an optimization process, are called *the outer nodes*, and the nodes defining the plane elements are called *the inner nodes*. The displacement vectors of the outer nodes and the inner nodes of the ith patch are denoted by ${}^{t+\Delta t}\mathbf{u}^{(k)}_{e,\text{out}}$ and ${}^{t+\Delta t}\mathbf{u}^{(k)}_{e,i,\text{in}}$ in the kth Newton–Raphson iteration, respectively. Therefore, the displacement update in the standard Newton–Raphson iteration is as follows:

$$\begin{bmatrix} {}^{t+\Delta t}\mathbf{u}^{(k)}_{e,\text{out}} \\ {}^{t+\Delta t}\mathbf{u}^{(k)}_{e,1,\text{in}} \\ \vdots \\ {}^{t+\Delta t}\mathbf{u}^{(k)}_{e,nl,\text{in}} \end{bmatrix} = \begin{bmatrix} {}^{t+\Delta t}\mathbf{u}^{(k-1)}_{e,\text{out}} \\ {}^{t+\Delta t}\mathbf{u}^{(k-1)}_{e,1,\text{in}} \\ \vdots \\ {}^{t+\Delta t}\mathbf{u}^{(k-1)}_{e,nl,\text{in}} \end{bmatrix} + \begin{bmatrix} \Delta\mathbf{u}^{(k)}_{e,\text{out}} \\ \Delta\mathbf{u}^{(k)}_{e,1,\text{in}} \\ \vdots \\ \Delta\mathbf{u}^{(k)}_{e,nl,\text{in}} \end{bmatrix} \tag{5}$$

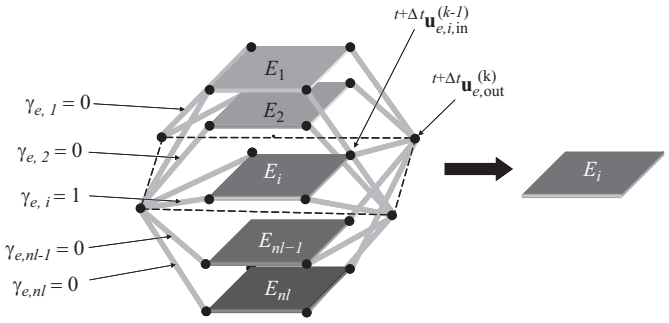

Fig. 4. Selecting the ith element at the eth patch using the design variables.

where $\Delta\mathbf{u}^{(k)}_{e,\text{out}}$ and $\Delta\mathbf{u}^{(k)}_{e,i,\text{in}}$ denote the updated displacements for the outer nodes and the inner nodes of the ith solid element at the eth patch, respectively, and are calculated by the following nonlinear static equation:

$$\mathbf{k}_{I,i,e} = l_{e,i}(\gamma_{e,1},\gamma_{e,2},\ldots,\gamma_{e,nl-1},\gamma_{e,nl})\mathbf{I}_{8\times 8} \quad (\text{where } \mathbf{I}_{8\times 8} \text{ is a } 8\times 8 \text{ identity matrix}) \tag{6}$$

$$\left\{ \begin{bmatrix} \sum_{j=1}^{nl}\mathbf{k}_{I,j,e} & -\mathbf{k}_{I,1,e} & \cdots & -\mathbf{k}_{I,nl,e} \\ -\mathbf{k}_{I,1,e} & \mathbf{k}_{I,1,e} & \cdots & \vdots \\ \vdots & \vdots & \ddots & \mathbf{0} \\ -\mathbf{k}_{I,nl,e} & \cdots & \mathbf{0} & \mathbf{k}_{I,nl,e} \end{bmatrix} + \begin{bmatrix} \mathbf{0} & \mathbf{0} & \mathbf{0} & \mathbf{0} \\ \mathbf{0} & {}^{t}\mathbf{k}^{structure,(k-1)}_{T,1,e} & \mathbf{0} & \mathbf{0} \\ \mathbf{0} & \mathbf{0} & \ddots & \mathbf{0} \\ \mathbf{0} & \mathbf{0} & \mathbf{0} & {}^{t}\mathbf{k}^{structure,(k-1)}_{T,nl,e} \end{bmatrix} \right\} \begin{bmatrix} \Delta\mathbf{u}^{(k)}_{e,\text{out}} \\ \Delta\mathbf{u}^{(k)}_{e,1,\text{in}} \\ \vdots \\ \Delta\mathbf{u}^{(k)}_{e,nl,\text{in}} \end{bmatrix} = \begin{bmatrix} \mathfrak{R}^{(k-1)}_{e,\text{out}} \\ \mathfrak{R}^{(k-1)}_{e,1,\text{in}} \\ \vdots \\ \mathfrak{R}^{(k-1)}_{e,nl,\text{in}} \end{bmatrix} \tag{7}$$

The first and second stiffness matrix terms of Eq. (7) are driven for the zero-length links and the plane elements of the eth patch, respectively. The stiffness value for the links of the ith solid element of the eth patch, $l_{e,i}$, is a function of the design variables ($\boldsymbol{\gamma}$). As a notation convention, the design variable for the ith solid element of the eth patch is denoted by $\gamma_{e,i}$. The stiffness matrix and the residual force terms of the outer and the inner nodes for the ith solid element of the eth patch are denoted by ${}^{t}\mathbf{k}^{structure,(k-1)}_{T,e}$, $\mathfrak{R}^{(k-1)}_{e,\text{out}}$, and $\mathfrak{R}^{(k-1)}_{e,i,\text{in}}$, respectively. For a special case, the above equation can be summarized as follows for the case of two layers:

$$\left\{ \begin{bmatrix} \mathbf{k}_{I,1,e}+\mathbf{k}_{I,2,e} & -\mathbf{k}_{I,1,e} & -\mathbf{k}_{I,2,e} \\ -\mathbf{k}_{I,1,e} & \mathbf{k}_{I,1,e} & \mathbf{0} \\ -\mathbf{k}_{I,2,e} & \mathbf{0} & \mathbf{k}_{I,2,e} \end{bmatrix} + \begin{bmatrix} \mathbf{0} & \mathbf{0} & \mathbf{0} \\ \mathbf{0} & {}^{t}\mathbf{k}^{structure,(k-1)}_{T,1,e} & \mathbf{0} \\ \mathbf{0} & \mathbf{0} & {}^{t}\mathbf{k}^{structure,(k-1)}_{T,2,e} \end{bmatrix} \right\} \begin{bmatrix} \Delta\mathbf{u}^{(k)}_{e,\text{out}} \\ \Delta\mathbf{u}^{(k)}_{e,1,\text{in}} \\ \Delta\mathbf{u}^{(k)}_{e,2,\text{in}} \end{bmatrix} = \begin{bmatrix} \mathfrak{R}^{(k-1)}_{e,\text{out}} \\ \mathfrak{R}^{(k-1)}_{e,1,\text{in}} \\ \mathfrak{R}^{(k-1)}_{e,2,\text{in}} \end{bmatrix} (nl=2) \tag{8}$$

To select no patch or one patch among several presented patches, it is important to derive appropriate interpolation functions of the employed zero-length links. In other words, it becomes essential to devise proper interpolation functions for selecting the ith element at the eth patch for which $\gamma_{e,i}=1$ (and zeros for all others), as shown in Fig. 4. This issue will be dealt with in Section 3.

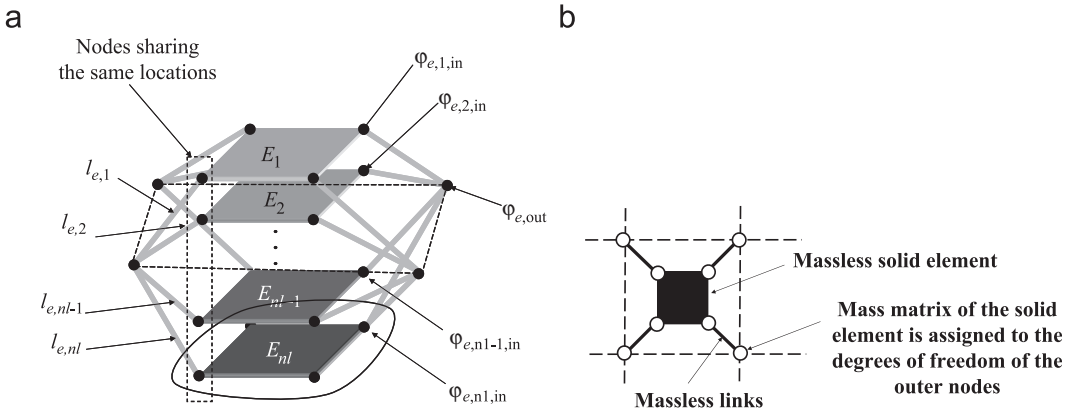

Fig. 5. (a) Patches in the patch stacking method and (b) concept of the patch mass model.

The residual forces $\Re_{e,\text{out}}^{(k-1)}$ and $\Re_{e,i,\text{in}}^{(k-1)}$ can be formulated as

$$\begin{bmatrix} \Re_{e,\text{out}}^{(k-1)} \\ \Re_{e,1,\text{in}}^{(k-1)} \\ \vdots \\ \Re_{e,nl,\text{in}}^{(k-1)} \end{bmatrix} = \begin{bmatrix} {}^{t+\Delta t}\mathbf{R}_e \\ \mathbf{0} \\ \mathbf{0} \\ \mathbf{0} \end{bmatrix} - \begin{bmatrix} \mathbf{0} \\ {}^{t+\Delta t}_{0}\mathbf{f}_{1,e}^{structure,(k-1)} \\ \vdots \\ {}^{t+\Delta t}_{0}\mathbf{f}_{nl,e}^{structure,(k-1)} \end{bmatrix} - \begin{bmatrix} \sum_{j=1}^{nl} {}^{t+\Delta t}_{0}\mathbf{f}_{e,j,\text{out}}^{link,(k-1)} \\ {}^{t+\Delta t}_{0}\mathbf{f}_{e,1,\text{in}}^{link,(k-1)} \\ \vdots \\ {}^{t+\Delta t}_{0}\mathbf{f}_{e,nl,\text{in}}^{link,(k-1)} \end{bmatrix} \tag{9}$$

where

$$\begin{bmatrix} {}^{t+\Delta t}_{0}\mathbf{f}_{e,j,\text{out}}^{link,(k-1)} \\ {}^{t+\Delta t}_{0}\mathbf{f}_{e,j,\text{in}}^{link,(k-1)} \end{bmatrix} = \begin{bmatrix} \mathbf{k}_{I,j,e} & -\mathbf{k}_{I,j,e} \\ -\mathbf{k}_{I,j,e} & \mathbf{k}_{I,j,e} \end{bmatrix} \begin{bmatrix} {}^{t+\Delta t}\mathbf{u}_{e,j,\text{out}}^{(k-1)} \\ {}^{t+\Delta t}\mathbf{u}_{e,j,\text{in}}^{(k-1)} \end{bmatrix} \quad (j=1,\cdots,nl) \tag{10}$$

In Eq. (9), the externally applied force on the outer nodes and the internal force of the ith plane element acting on the inner nodes are denoted by ${}^{t+\Delta t}\mathbf{R}$ and ${}^{t}_{0}+\Delta t\mathbf{f}_{i,e}^{structure,(k-1)}$, respectively.

Compared with the number of nodes in the standard density-based topology optimization scheme, the number of nodes used in the ECP method is quite a bit larger than the number of nodes used in the element density-based method. When we consider the example in Fig. 1, the number of nodes of the ECP patch is $nl\times 4+4$, whereas the number of nodes in the density method is 4. Thus, the static condensation scheme was proposed in Ref. [16] in order to reduce the size of the global stiffness matrix and the associated computational times. In other words, because the degrees of freedom of the inner nodes of one patch are independent of those of the inner nodes of other neighboring patches, they can be statically condensed out from the global stiffness matrix as follows:

$$\left\{ \begin{bmatrix} \sum_{j=1}^{nl}\mathbf{k}_{I,j,e} & -\mathbf{k}_{I,1,e} & \cdots & -\mathbf{k}_{I,nl,e} \\ -\mathbf{k}_{I,1,e} & \mathbf{k}_{I,1,e}+{}^{t}\mathbf{k}_{T,1,e}^{structure,(k-1)} & \cdots & \vdots \\ \vdots & \vdots & \ddots & \mathbf{0} \\ -\mathbf{k}_{I,nl,e} & \cdots & \mathbf{0} & \mathbf{k}_{I,nl,e}+{}^{t}\mathbf{k}_{T,nl,e}^{structure,(k-1)} \end{bmatrix} - \omega^2 \begin{bmatrix} \sum_{j=1}^{nl}\mathbf{m}_{j,e} & \cdots & \mathbf{0} \\ \vdots & \ddots & \vdots \\ \mathbf{0} & \cdots & \mathbf{0} \end{bmatrix} \right\} \begin{bmatrix} \Delta\mathbf{u}_{e,\text{out}}^{(k)} \\ \Delta\mathbf{u}_{e,1,\text{in}}^{(k)} \\ \vdots \\ \Delta\mathbf{u}_{e,nl,\text{in}}^{(k)} \end{bmatrix} = \begin{bmatrix} \Re_{e,\text{out}}^{(k-1)} \\ \Re_{e,1,\text{in}}^{(k-1)} \\ \vdots \\ \Re_{e,nl,\text{in}}^{(k-1)} \end{bmatrix} \tag{16}$$

$$\begin{aligned} {}^{t}\mathbf{k}_{Con,e}^{(k-1)} &= \left(\sum_{j=1}^{nl}\mathbf{k}_{I,j,e} - \sum_{j=1}^{nl}[\mathbf{k}_{I,j,e}(\mathbf{k}_{I,j,e}+{}^{t+\Delta t}\mathbf{k}_{T,j,e}^{structure,(k-1)})^{-1}\mathbf{k}_{I,j,e}]\right) \\ &= \sum_{j=1}^{nl}[\mathbf{k}_{I,j,e} - \mathbf{k}_{I,j,e}(\mathbf{k}_{I,j,e}+{}^{t+\Delta t}\mathbf{k}_{T,j,e}^{structure,(k-1)})^{-1}\mathbf{k}_{I,j,e}] \\ &\quad \text{(from equation (7))} \end{aligned} \tag{11}$$

$${}^{t}\mathbf{k}_{Con,e}^{(k-1)}\Delta\mathbf{u}_{e,\text{out}}^{(k)} = \Re_{e,\text{out}}^{(k-1)} + \sum_{j=1}^{nl}(\mathbf{k}_{I,j,e}(\mathbf{k}_{I,j,e}+{}^{t}\mathbf{k}_{T,j,e}^{structure,(k-1)})^{-1}\Re_{e,j,\text{in}}^{(k-1)}) \tag{12}$$

where the condensed stiffness matrix of the eth patch is denoted by ${}^{t}\mathbf{k}_{Con,e}^{(k-1)}$. Then, the global tangent stiffness matrix is assembled as

$${}^{t}\mathbf{K}_{Con}^{(k-1)} = \mathop{\mathrm{A}}_{e=1}^{N_p} {}^{t}\mathbf{k}_{Con,e}^{(k-1)} \tag{13}$$

where N_p is the total number of patches. With the help of the above static condensation scheme, the number of degrees of freedom of the condensed stiffness matrix ${}^{t}\mathbf{K}_{Con}^{(k-1)}$ becomes the same as that of the stiffness matrix of the standard element density method. Finally, the following system of equations is solved iteratively for $\Delta\mathbf{U}_{\text{out}}^{(k)}$, which is the global updated displacement vector for the outer nodes:

$${}^{t}\mathbf{K}_{Con}^{(k-1)}\Delta\mathbf{U}_{\text{out}}^{(k)} = \Re_{Con}^{(k-1)} \tag{14}$$

where

$$\Re_{Con}^{(k-1)} = \Re_{e,\text{out}}^{(k-1)} + \sum_{j=1}^{nl}(\mathbf{k}_{I,j,e}(\mathbf{k}_{I,j,e}+{}^{t}\mathbf{k}_{T,j,e}^{structure,(k-1)})^{-1}\Re_{e,j,\text{in}}^{(k-1)}) \tag{15}$$

The displacements of the inner nodes can be calculated from Eq. (7).

2.2.3. Nonlinear dynamic equation

As observed in the eigenfrequency optimization problem in the density-based optimization procedure, localized vibrating modes are observed in the ECP method. Furthermore, the localized vibrating modes between the outer nodes and the inner nodes are additionally observed in the ECP method. To resolve the localized modes within patches (see Ref. [9] for more details), this paper utilizes the patch mass matrix presented in Ref. [9], which is a new concept that assembles the mass matrices of the solid elements in patches into the degrees of freedom of the outer nodes, as shown in Fig. 5(b). Unlike the straightforward method of assigning the mass stiffness matrices to the degrees of freedom of the inner nodes, the solid elements of the patch are modeled as massless, which makes the eigenfrequencies between the inner and the outer nodes numerically infinite. After employing this patch mass matrix approach, the eigenvalue problem is formulated as follows:

As we did for the stiffness matrix, the following condensation scheme is applied for the global mass matrix

$$\mathbf{M}_{Con} = \mathop{\mathrm{A}}_{e=1}^{N_p}\sum_{j=1}^{nl}\mathbf{m}_{j,e} \tag{17}$$

Finally, the following modal equation is solved in order to obtain the eigenmodes of the outer nodes, $\mathbf{\Phi}_{out}$.

$$[{}^{t}\mathbf{K}_{Con}-\omega^2\mathbf{M}_{Con}]\mathbf{\Phi}_{out} = \mathbf{0} \tag{18}$$

where ${}^{t}\mathbf{K}_{Con}$ is the converged tangent stiffness matrix after several iterations in Eq. (14).

3. Topology optimization formulation

3.1. Material interpolation: stiffness matrix and mass matrix

As stated, in the present patch stacking method, it is a vital to devise proper interpolation functions for a mass matrix as well as stiffness values of the links in order to make the design variables converge to zero or one. Element selection formulations proposed by other researchers can be used for the stiffness values [1], and it is found here that careful consideration is required in devising the

interpolation functions for a mass matrix with respect to the design variable.

3.1.1. Interpolation function for link stiffness

In the ECP-based approach, it was known that special interpolation functions are required (see Refs. [9,17] for details). Therefore, it becomes an issue to make interpolation functions for multiple materials as well. Therefore, the following interpolation functions were newly devised:

$$l_{e,i} = \alpha \frac{\xi_{e,i}}{1+(1-\xi_{e,i})\tau} + \beta \quad \left(\tau = \frac{\alpha \times s}{k^{structure}_{diagonal,small} \times k}\right) \tag{19}$$

$$\xi_{e,i} = (1-\gamma_{e,1})^n \cdots (1-\gamma_{e,i-1})^n (\gamma_{e,i})^n (1-\gamma_{e,i+1})^n \cdots (1-\gamma_{e,nl})^n \tag{20}$$

$$\alpha = l_{\max} - l_{\min}, \beta = l_{\min} \tag{21}$$

$$\gamma_{\min} \le \gamma_e \le 1, \quad \gamma_{\min} = 0.001 \tag{22}$$

where the link stiffness for the ith layer of the eth patch is $l_{e,i}$ and the associated auxiliary variable is $\xi_{e,i}$, which is the interpolation function of the SIMP method for multiple materials. To determine $l_{\max}$ and $l_{\min}$ consistently, the minimum diagonal stiffness value among those of the stiffness matrices for multiple materials is chosen for $k^{structure}_{diagonal,small}$: Testing other diagonal values produces similar layouts. The number of degrees of freedom per node is k. Here, $l_{\max}$ and $l_{\min}$ are set to $10^6 \times k^{structure}_{diagonal}$ and $10^{-6} \times k^{structure}_{diagonal}$, respectively. We set $n=3$, $k=2$, and $s=10$ because optimal layouts similar to those obtained in the solid isotropic material with penalization (SIMP) method could be obtained. For two layers, the above interpolation is summarized as follows.

For 2 layers:

$$l_{e,1} = \alpha \frac{\xi_{e,1}}{1+(1-\xi_{e,1})\tau} + \beta, \quad l_{e,2} = \alpha \frac{\xi_{e,2}}{1+(1-\xi_{e,2})\tau} + \beta$$
$$\xi_{e,1} = (\gamma_{e,1})^n (1-\gamma_{e,2})^n, \quad \xi_{e,2} = (1-\gamma_{e,1})^n (\gamma_{e,2})^n \tag{23}$$

To understand the above interpolation functions for two layers, Table 1 summarizes the physical meanings for each case.

One interesting observation in Table 1 is that the first and second patches become voids with 1 for $\gamma_{e,1}$ and $\gamma_{e,2}$.

3.1.2. Interpolation function 1 for mass matrix

Like the stiffness interpolation function, the mass interpolation function for the present patch stacking method can be constructed as follows; in fact, they are constructed from Eq. (23) without the penalty n

$$\mathbf{m}_{i,e} = \mathbf{m}_{i,orgin}\{(1-\gamma_{e,1}) \cdots (1-\gamma_{e,i-1})\gamma_{e,i-1}(1-\gamma_{e,i+1}) \cdots (1-\gamma_{e,nl})\} \tag{24}$$

where the $\mathbf{m}_{i,orgin}$ is the mass matrix of the ith solid element. For the case of two layers, the above equation can be summarized as

$$\mathbf{m}_{e,1} = \mathbf{m}_{1,orgin}\gamma_{e,1} \times (1-\gamma_{e,2}) \tag{25}$$

$$\mathbf{m}_{e,2} = \mathbf{m}_{2,orgin}(1-\gamma_{e,1}) \times \gamma_{e,2} \tag{26}$$

Table 1
Physical meanings of the interpolation functions of Eq. (23).

$\gamma_{e,1}$	$\gamma_{e,2}$	Physical meaning of the first layer/$l_{e,1}$	Physical meaning of the second layer/$l_{e,2}$
1	1	Non-structure/β	Non-structure/β
1	0	Structure/α	Non-structure/β
0	1	Non-structure/β	Structure/α
0	0	Non-structure/β	Non-structure/β

Table 2
First mass model for two layers.

$\gamma_{e,1}$	$\gamma_{e,2}$	First layer	Second layer
1	1	*Non-structure*	*Non-structure*
1	0	Structure	Non-structure
0	1	Non-structure	Structure
0	0	Non-structure	Non-structure

Table 3
Second mass model for two layers.

$\gamma_{e,1}$	$\gamma_{e,2}$	First layer	Second layer
1	1	*Structure*	*Structure*
1	0	Structure	Non-structure
0	1	Non-structure	Structure
0	0	Non-structure	Non-structure

To make it clear, Table 2 summarizes the physical status of the above mass model. From here, it is understood that because we employed the concept of the interpolation function of the stiffness matrix, the physical status are same as those of the stiffness interpolation functions.

Although the interpolation functions of Eqs. (25) and (26) are easy and straightforward to understand, it is empirically found that the mass interpolations create highly localized modes and numerical difficulties in optimization with a larger move limit. For example, consider some patches that have ones for all associated design variables. Because these patches have void properties for stiffness and mass, they cannot be distinguished from other patches with zeros for all associated design variables. For these reasons, an optimization algorithm can take advantage of this side effect in finding optimal layouts. This feature will be illustrated in the numerical example section.

3.1.3. Interpolation function 2 for mass matrix: separable mass matrix

To resolve the numerical side effect of the first mass interpolation function, we modify the mass matrix interpolation functions by adding an extra term, as follows:

$$\mathbf{m}_{i,e} = \mathbf{m}_{i,orgin}\{(1-\gamma_{e,1}) \cdots (1-\gamma_{e,i-1})\gamma_{e,i-1}(1-\gamma_{e,i+1}) \cdots (1-\gamma_{e,nl}) + \gamma^n_{e,1}\gamma^n_{e,2} \cdots \gamma^n_{e,nl-1}\gamma^n_{e,nl}\} \tag{27}$$

For two layers:

$$\mathbf{m}_{e,1} = \mathbf{m}_{1,orgin}(\gamma_{e,1} \times (1-\gamma_{e,2}) + \gamma^n_{e,1}\gamma^n_{e,2}) \tag{28}$$

$$\mathbf{m}_{e,2} = \mathbf{m}_{2,orgin}((1-\gamma_{e,1}) \times \gamma_{e,2} + \gamma^n_{e,1}\gamma^n_{e,2}) \tag{29}$$

Table 3 summarizes the physical status of the above interpolation function in order to compare the first interpolation functions for the case of two layers. As shown, because $\mathbf{m}_{e,1}$ and $\mathbf{m}_{e,2}$ have $\mathbf{m}_{1,orgin}$ and $\mathbf{m}_{2,orgin}$ for ones for $\gamma_{e,1}$ and $\gamma_{e,2}$, the corresponding areas will have lower eigenfrequencies, which is uneconomical. Therefore, an optimization algorithm will not make ones for the two design variables.

3.1.4. An elementary example

To verify the proposed material interpolation functions, we consider a simpler example in Fig. 6. Young's modulus of the first layer is twice as large as that of the second layer, while the mass density of the first layer is half that of the second layer. To understand the effect of the interpolation functions of Eqs. (24) and (27), the first eigenfrequency of the system is plotted with the two interpolation functions. As shown, the interpolation function (27) shows more convex functional space. Furthermore, it

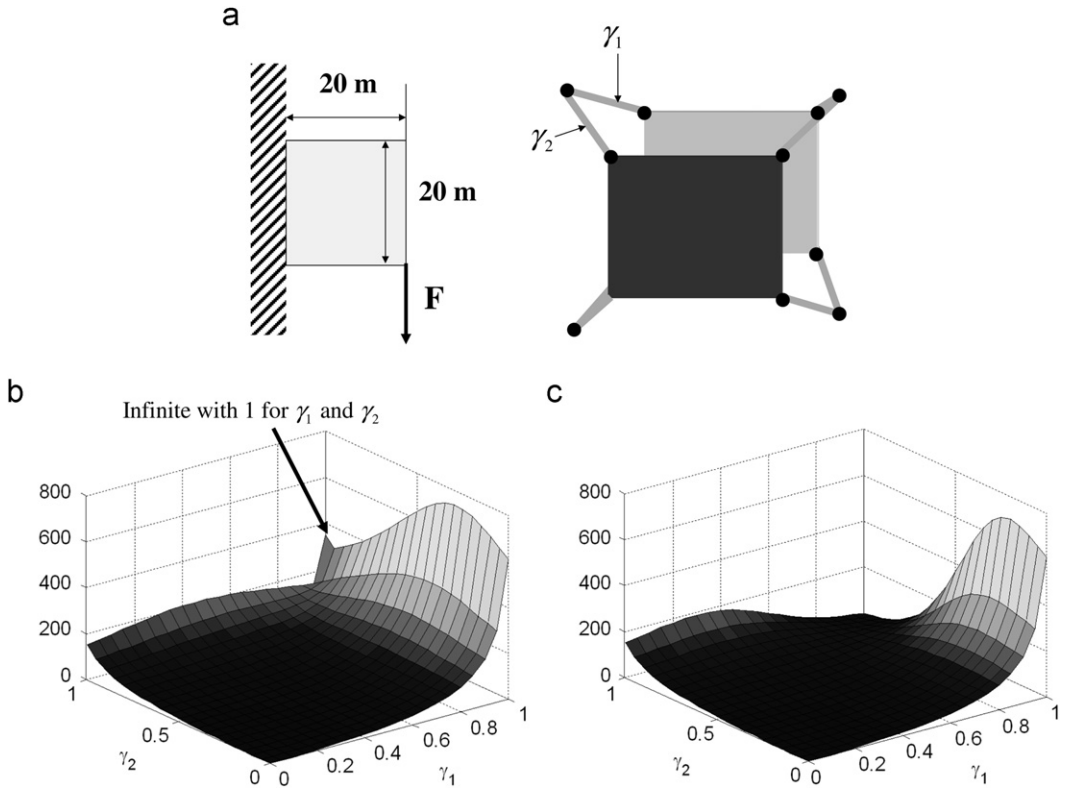

Fig. 6. An elementary example of the interpolation function. (a) Definition of problem definition, (b) frequency curve with the first interpolation function, and (c) frequency curve with the second interpolation function.

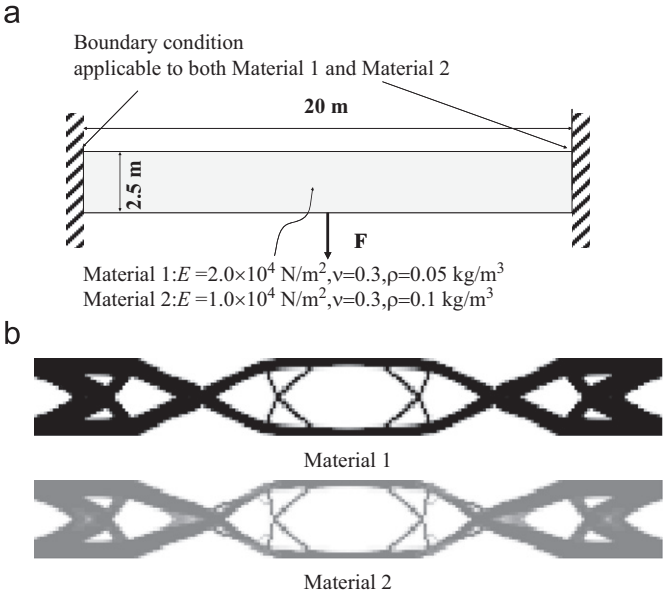

Fig. 7. Definition of the problem of a rectangular box with two materials. (a) The geometry and the boundary condition and (b) optimized layouts using either material 1 or material 2 using only linear strain analysis.

shows that within the functional space there are more than three local optima. Thus, it cannot be guaranteed that the proposed layouts will be far from the global optima.

3.2. Topology optimization formulation

For the sake of simplicity, we consider topology optimization to maximize only the fundamental eigenfrequency of a geometrically nonlinear structure, which is defined as

$$\begin{aligned}
&\underset{\boldsymbol{\gamma}}{\text{Max}} \left\{ \underset{j=1,\ldots,J}{\text{Min}} \{\omega_j\} \right\} \\
&\text{s.t.} \quad \sum_{e=1}^{N_p} \rho_e(\gamma_{e,i}) \mathrm{v}_{e,i} \le V_i^* \quad (i = 1, \cdots, nl) \\
&\qquad \Re({}^{\mathrm{t}+\Delta\mathrm{t}}\mathbf{U}) = \mathbf{0} \\
&\qquad ({}^{\mathrm{t}+\Delta\mathrm{t}}\mathbf{K}({}^{\mathrm{t}+\Delta\mathrm{t}}\mathbf{U}) - \omega^2\mathbf{M})\boldsymbol{\Phi} = \mathbf{0}
\end{aligned} \tag{30}$$

where ρ_e, $\mathrm{v}_{e,i}$, and V_i^* are the element density, element volume, and prescribed volume limit for the ith material, respectively. The converged displacements obtained by solving the nonlinear static equation are denoted by ${}^{\mathrm{t}+\Delta\mathrm{t}}\mathbf{U}^*$, and the number of candidate eigenfrequencies is denoted by J. To determine optimal topologies using a gradient-based optimizer, the sensitivity analysis of the jth eigenfrequency, ω_j, should be performed with respect to the design variable. By differentiating the equation of modal analysis equation, the following sensitivity equation can be derived for the patch mass method (see Ref. [9]):

$$\frac{d\omega_j}{d\gamma_{e,i}} = \sum_{k=1}^{nl} \frac{1}{2\omega_j} \times \left((\boldsymbol{\varphi}_{e,\mathrm{out}} - \boldsymbol{\varphi}_{e,k,\mathrm{in}})^{\mathrm{T}} \frac{dl_{e,k}}{d\gamma_{e,i}} (\boldsymbol{\varphi}_{e,\mathrm{out}} - \boldsymbol{\varphi}_{e,k,\mathrm{in}}) - \omega_j^2 \boldsymbol{\varphi}_{e,\mathrm{out}}^{\mathrm{T}} \frac{d\mathbf{m}_{e,k}}{d\gamma_{e,i}} \boldsymbol{\varphi}_{e,\mathrm{out}} \right) \tag{31}$$

For two layers:

$$\frac{d\omega_j}{d\gamma_{e,i}} = \frac{1}{2\omega_j} \times \left(\begin{array}{l} (\boldsymbol{\varphi}_{e,\mathrm{out}} - \boldsymbol{\varphi}_{e,1,\mathrm{in}})^{\mathrm{T}} \frac{dl_{e,1}}{d\gamma_{e,i}} (\boldsymbol{\varphi}_{e,\mathrm{out}} - \boldsymbol{\varphi}_{e,1,\mathrm{in}}) - \omega_j^2 \boldsymbol{\varphi}_{e,\mathrm{out}}^{\mathrm{T}} \frac{d\mathbf{m}_{e,1}}{d\gamma_{e,i}} \boldsymbol{\varphi}_{e,\mathrm{out}} \\ + (\boldsymbol{\varphi}_{e,\mathrm{out}} - \boldsymbol{\varphi}_{e,2,\mathrm{in}})^{\mathrm{T}} \frac{dl_{e,2}}{d\gamma_{e,i}} (\boldsymbol{\varphi}_{e,\mathrm{out}} - \boldsymbol{\varphi}_{e,2,\mathrm{in}}) - \omega_j^2 \boldsymbol{\varphi}_{e,\mathrm{out}}^{\mathrm{T}} \frac{d\mathbf{m}_{e,2}}{d\gamma_{e,i}} \boldsymbol{\varphi}_{e,\mathrm{out}} \end{array} \right)$$

4. Topology optimization examples

To show the potential use of the present optimization formulation, this section provides several numerical examples that are difficult to solve in the framework of the standard

optimization formulation. The key to topology optimization is the use of a proper optimization algorithm. In this research, we employ the method of moving asymptotes for a topology optimization algorithm written in the framework of MATLAB [18]. The analysis code is also implemented in the framework of MATLAB. For the present numerical examples, the design domains and material properties are arbitrarily chosen in order to show the potential of the present patch stacking schemes in topology optimization.

4.1. Example 1: rectangular box with two materials

First, we consider the topology optimization problem in Fig. 7 with **F**=0 N, which does not cause nonlinear strain with two materials. Young's modulus and the density with the first material are two-and-a-half times and half of those of the second material, respectively, as described in Fig. 7(a). By controlling the mass limits in Eq. (30), i.e., 50% for the first material and 0% for the second material in Fig. 7(b), and vice versa, optimized layouts are obtained that are similar to linear optimization layouts for either material 1 or material 2 in Fig. 7. By setting the design variables of either the first or the second layers to zero, the interpolation functions in (24) and (27) become the same interpolation function for the topology optimization for one material. For the sake of illustration, the first material is rendered as black while the second material is rendered as gray.

To test the effects of the material interpolation function for a mass matrix, the previous optimization problem is resolved using the two interpolation functions in Eqs. (24) and (27). Because of the abovementioned side effect of Eq. (24) in Table 1, there are some areas, marked by circles in Fig. 8(a), with two materials. This side effect also results in wobbly optimization iterations, but by employing the interpolation function in Eq. (27), a result whose outline is similar to the results in Fig. 7(b) is obtained. Therefore, unless stated otherwise, the second interpolation function will be used for the rest of our examples.

Next, we solve the topology optimization problem considering the geometrical nonlinearity in Fig. 9 with different magnitudes of the force **F**. It can be understood at a glance that the obtained designs in Fig. 9 are very similar to the designs with a single material [9]. From these results, it seems that the statement that a similar result of a compliance minimization problem can be obtained by maximizing the first eigenfrequency is also applicable in case of topology optimization with multiple materials. Fig. 12(a) shows the frequency curves of each design with various magnitudes of the force **F**. A comparison of the frequencies in each design indicates that the designs that consider geometrical nonlinearity have larger first eigenfrequencies. Furthermore, as one of the limitations, unfortunately we also can recognize that the designs in Fig. 11 are not optimized for the given loads; the design with 5 N is superior even for other magnitudes of load, in terms of the eigenfrequency of interest. From these observations, it is understood that the obtained and presented designs are local optima. From a physical point of view, we understand that the

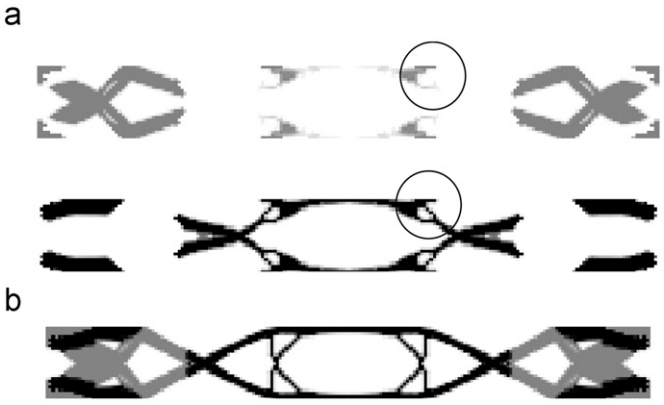

Fig. 8. Optimized layouts with (a) the material interpolation of Eq. (24) and (b) the material interpolation of Eq. (27).

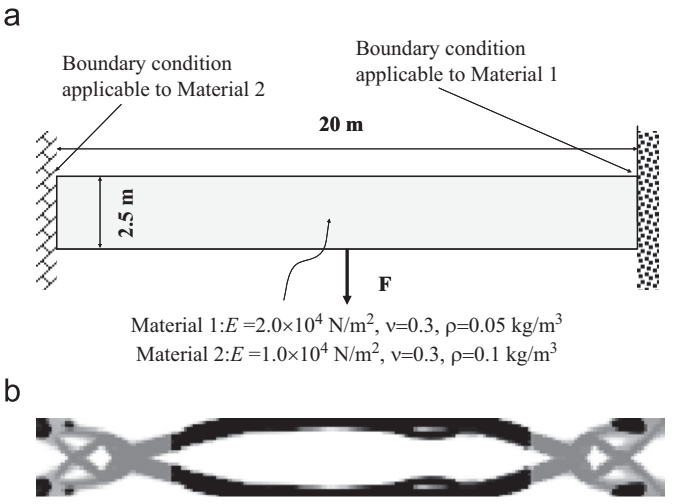

Fig. 10. Definition of the problem of a rectangular box using two materials with the prescribed material-dependent boundary condition. (a) The geometry and the boundary condition and (b) the result obtained by linear analysis.

Fig. 9. Optimization results with a homogeneous boundary condition (clamp conditions for both materials). (a) The obtained result with **F**=2.5 N, (b) with **F**=5 N, and (c) with **F**=10 N.

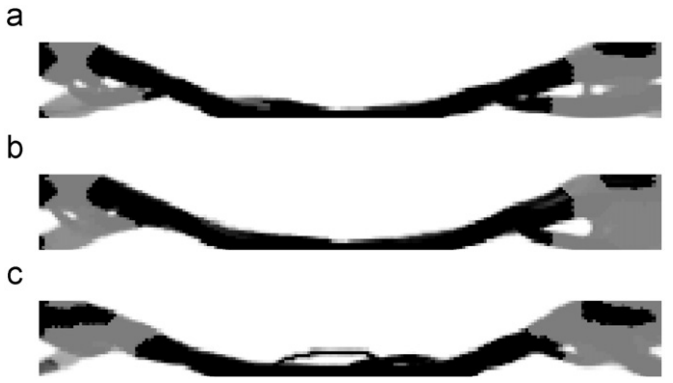

Fig. 11. Nonlinear optimization results with the material-dependent boundary condition for the problem in Fig. 10. (a) The optimized result with **F**=2.5 N, (b) with **F**=5 N, and (c) with **F**=10 N.

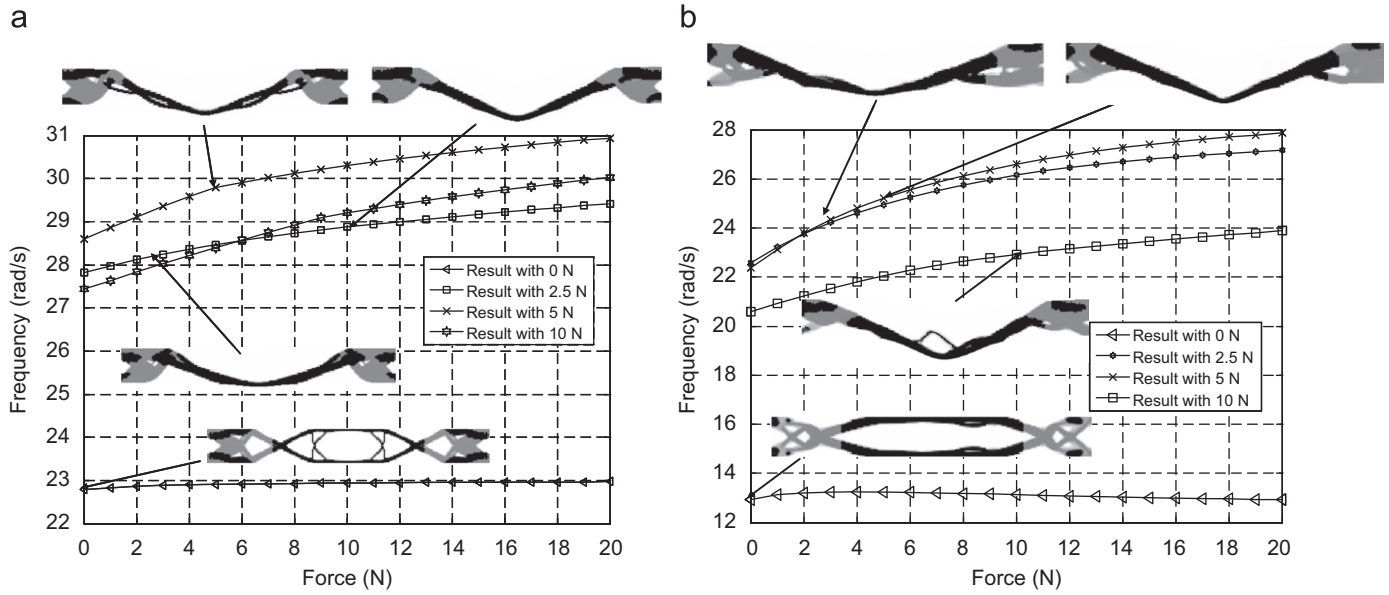

Fig. 12. Load and frequency curves. (For purpose of illustration, the deformations of structures are scaled by a factor 10). (a) Curves for the designs of Figs. 8 and 10 and (b) curves for the designs of Figs. 10 and 11.

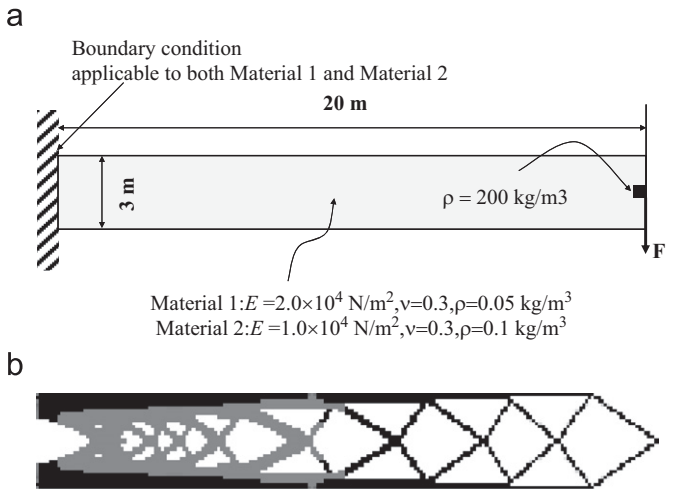

Fig. 13. Definition of the problem of a rectangular box with two materials with the material-independent boundary condition. (a) Definition of the problem and (b) the optimized layout.

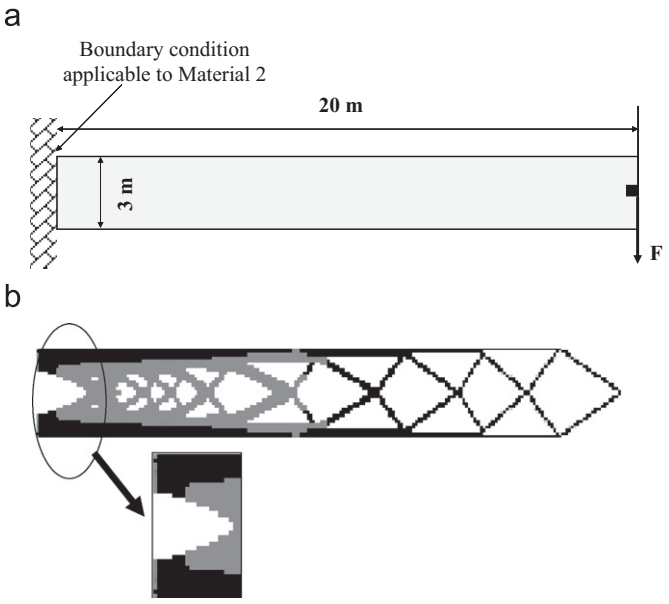

Fig. 14. Definition of the problem of a rectangular box using two materials with the material-dependent boundary condition. (a) The geometry and the boundary condition and (b) the results obtained by linear analysis.

issue of local optima becomes serious in the considered problems due to the bifurcation of intermediate designs and the heuristic interpolation schemes. In order to resolve this local optima issue, we may either start with different initial solutions or adopt a global optimizer such as a genetic algorithm.

In Fig. 10, the material-dependent boundary condition is tested with no zero forces causing the geometrical nonlinearity. The left and the right boundaries of the design domain are clamped only for the second material and the first material, respectively. To implement the material-dependent boundary condition, the new nodes are inserted at these sides and the connectivity information of the elements located at these sides is modified, as shown in Fig. 10(a). Fig. 10 shows the optimized results with two materials. Due to the material-dependent boundary condition, vertically asymmetric designs are obtained. The geometric nonlinearity is considered in Fig. 11 and the asymmetric designs are obtained. Fig. 12 shows the load and the frequency curves of these designs. As in the previous examples, the obtained designs are local optima.

4.2. Example 2: beam structure with a point load

For the second optimization example, the beam structure with a point mass is considered in Fig. 13. Note that as this example with the point mass has been widely used to validate new schemes in topology optimization for dynamic problem, a thorough study of this structure with the present method can show some potential and limitations of the present method. The material properties of the problem are set the same as those in the first example. The domain is discretized by 200 by 25 patches and the point mass is attached at the end of the beam to avoid a trivial void structure. The linear design is shown in Fig. 13(b). Also, optimized layouts in this example are rendered in black for the first material and gray for the second material.

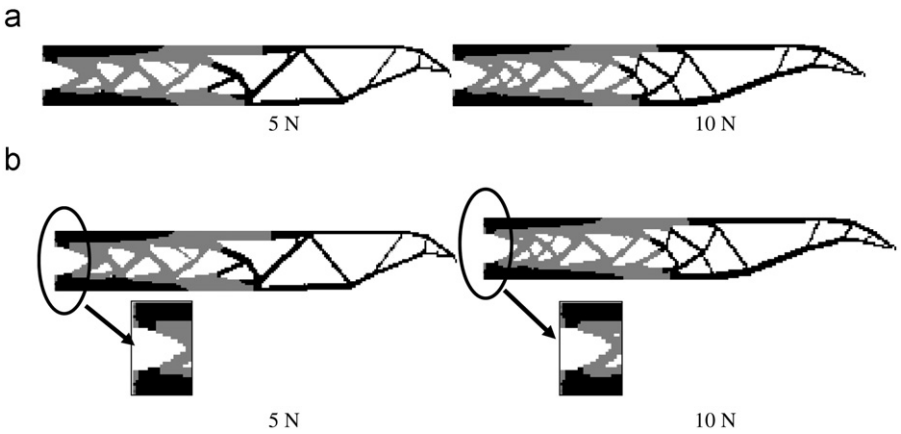

Fig. 15. Optimization results using both material 1 and material 2. (a) Obtained result with the clamped boundary condition for two materials and (b) obtained result with the clamp boundary condition only for the second material.

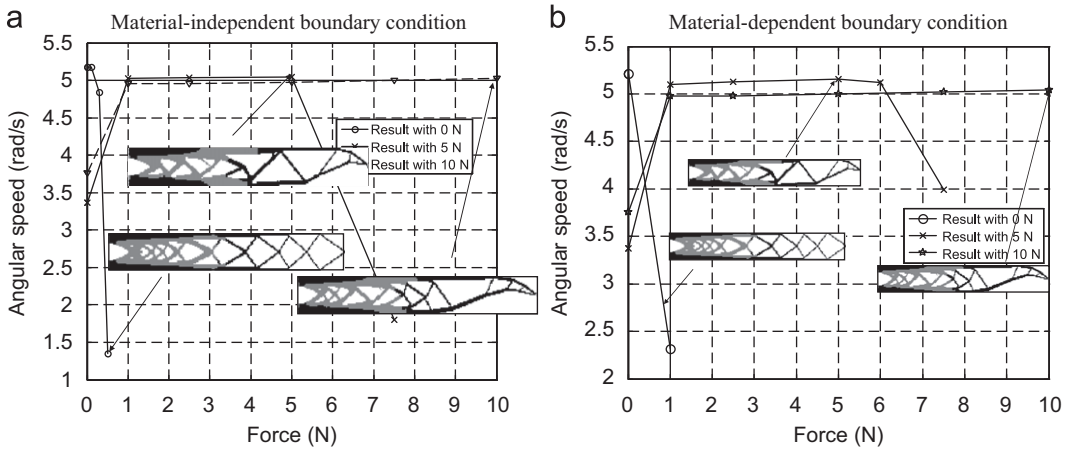

Fig. 16. Load and frequency curves. (a) Material-independent boundary condition and (b) material-dependent boundary condition.

Next, using linear analysis, the material-dependent boundary condition in Fig. 14 is considered. Unlike in the previous example, the clamp boundary condition on the left side is only applied to material 2. The optimized layout is presented in Fig. 14(b). As can be seen, the second material appears on the left side and the other parts of the layout are similar to those in the results in Fig. 13(b).

Fig. 15 shows the optimized results with the clamped boundary condition for two materials and the clamped boundary condition only for the second material for different point loads. As shown in Fig. 15(a), except for the fact that two materials are used, the optimized layouts are made similar to the layouts by minimizing the compliance considering the geometrical nonlinearity and by maximizing the first eigenfrequency with one material. Fig. 16 compares the eigenfrequencies of the obtained designs with respect to the applied loads. As illustrated in Fig. 16, in this particular example, the optimizer does not have any difficulty in obtaining the designs optimized for the given loads because the first eigenmode is the bending mode.

5. Conclusions

This paper develops a new scheme to solve the nonlinear eigenvalue problem considering multiple materials and the material-dependent boundary condition. When these problems are solved using the existing standard approaches to topology optimization, complicated issues may arise, such as unstable elements and the complicated reformulation of the optimization for the material-dependent boundary condition. In response to this, this paper presents a new patch stacking method based on the element connectivity parameterization (ECP) method, which is effective for the unstable elements. Unlike existing multi-material topology optimization schemes, the important differences in the proposed method are the stacking of multiple patches of the ECP method on the same discretization pixel and the selection of one patch or no patch. From the numerical examples, we find that the considered optimization problem suffers from the local optima. Therefore, the presented results are not the global optima. Also, it is observed that the layouts optimized for the first eigenvalue are similar to those that minimize the static compliance, even with multiple materials and material-dependent boundary conditions.

Acknowledgement

The author acknowledges the support from Basic Science Research Program through the National Research Foundation of Korea (NRF) funded by the Ministry of Education, Science and Technology (2010-0028152).

References

[1] M.P. Bendsøe, O. Sigmund, Topology Optimization Theory, Methods and Applications, Springer-Verlag, New York, 2003.
[2] C.S. Jog, Topology design of structures subjected to periodic loading, J. Sound Vib. 253 (3) (2002) 687–709.

[3] Z.D. Ma, N. Kikuchi, I. Hagiwara, Structural topology and shape optimization for a frequency response problem, Comput. Mech. 13 (3) (1993) 157–174.
[4] N.L. Pedersen, Maximization of eigenvalues using topology optimization, Struct. Multidisciplinary Optim. 20 (1) (2000) 2–11.
[5] T.S. Kim, Y.Y. Kim, Mac-based mode-tracking in structural topology optimization, Comput. Struct. 74 (2000) 375–383.
[6] J. Du, N. Olhoff, Topological design of freely vibrating continuum structures for maximum values of simple and multiple eigenfrequencies and frequency gaps, Struct. Multidisciplinary Optim. 34 (2007) 91–110.
[7] Y. Maeda, S. Nishiwaki, K. Izui, M. Yoshimura, K. Matsui, K. Terada, Structural topology optimization of vibrating structures with specified eigenfrequencies and eigenmode shapes, Int. J. Numer. Methods Eng. 67 (2006) 597–628.
[8] D. Tcherniak, Topology optimization of resonating structures using SIMP method, Int. J. Numer. Methods Eng. 54 (2002) 1605–1622.
[9] G.H. Yoon, Maximizing the fundamental eigenfrequency of geometrically nonlinear structures by topology optimization based on element connectivity parameterization, 88 (2010) 120–133.
[10] G.H. Yoon, J.S. Jensen, O. Sigmund, Topology optimization of acoustic–structure interaction problems using a mixed finite element formulation, Int. J. Numer. Method Eng. 70 (2007) 1049–1076.
[11] A.R. Diaz, N. Kikuchi, Solutions to shape and topology eigenvalue optimization using a homogenization method, Int. J. Numer. Method Eng. 35 (1992) 1487–1502.
[12] G.H. Yoon, Y.Y. Kim, Element connectivity parameterization for topology optimization of geometrically nonlinear structures, Int. J. Solids Struct. 42 (7) (2005) 1983–2009.
[13] G.H. Yoon, Y.K. Park, Y.Y. Kim, Element stacking method for topology optimization with material-dependent boundary and loading conditions, J. Mech. Mater. Struct. 2 (5) (2007) 883–895.
[14] K.J. Bathe, Finite element procedures, Prentice Hall, New Jersey, 1996.
[15] R.D. Cook, D.S. Malkus, M.E. Plesha, R.J. Witt, Concepts and applications of finite element analysis, 4th Edition, John Wiley & Sons, USA, 2001.
[16] G.H. Yoon, Y.S. Joung, Y.Y. Kim, Optimal layout design for three dimensional geometrical nonlinear structures using the element connectivity parameterization, Int. J. Numer. Methods Eng. 69 (2007) 1278–1304.
[17] G.H. Yoon, Y.Y. Kim, M. Langelaar, F.V. Keulen, Theoretical aspects of the internal element connectivity parameterization approach for topology optimization, Int. J. Numer. Method Eng. 76 (2002) 77–797.
[18] K. Svanberg, The method of moving asymptotes—a new method for structural optimization, Int. J. Numer. Methods Eng. 24 (1987) 359–373.